Hyperloop Communications: Intra-tube Channel Capacity and its Enhancement

Jeongtak Kim
Dept. of Electrical Engineering
UNIST, Ulsan, Korea
jtkim@unist.ac.kr

Hyoil Kim
Dept. of Electrical Engineering
UNIST, Ulsan, Korea
hkim@unist.ac.kr

Ki Jin Han
Division of Electronics and Electrical Engineering
Dongguk University, Seoul, Korea
kjhan@dongguk.edu

***Abstract*—Hyperloop is a futuristic transfortation system to carry passengers and frieght in the vehicle called 'pod', which travels at the speed of 1,200 km/h within a near-vacuum 'tube'. To ensure safety and to provide Internet connectivity to passengers, wireless communications is an essential building block whose development necessitates evaluating and enhancing intra-tube wireless channel capacity. In this regard, this paper presents an in-depth investigation of per-pod downlink channel capacity, leveraging our previously-developed novel evaluation methodology on intra-tube electromagnetic (EM) propagation characteristics. Specifically, we first show that metallic pods (as considered in most Hyperloop proposals) cannot satisfy the per-passenger capacity requirement for on-board Internet service. As a remedy, we propose a double-layered pod structure to enhance the channel capacity, consisting of an EM absorbing outer layer and a metallic inner layer enclosing the passenger cabin. Our intensive evaluations revealed that double-layered pods achieve per-pod channel capacity large enough to support 4K UHD video streaming for all the passengers, thanks to the outer layer absorbing the power of interference signals. Furthermore, we present how to maximize the channel capacity via an optimized thickness of the EM absorbing layer and the choice of the best EM mode for communications.**

***Index Terms*—Hyperloop, Shannon capacity, capacity analysis, EM mode, EM absorbing material**

I. INTRODUCTION

Hyperloop is next-generation land transportation with a near-sonic speed of 1200 km/h where a vehicle called *pod* carries passengers or freight by cruising in a near-vacuum *tube*. Since its concept was first introduced in 2013 [1], there have been much industrial effort to realize Hyperloop from various companies like SpaceX, Hardt Hyperloop, Virgin Hyperloop, Hyperloop Transportation Technologies (HTT), Transpod, etc. For example, SpaceX hosted the Hyperloop pod competition from 2015 to 2019, where a number of teams participated with their own prototype pods. In 2020, Virgin Hyperloop demonstrated the world's first passenger test with two people on board in a full-scale pod travelling at 160 km/h. In addition, HTT has revealed its full-scale passenger capsule in 2018 and its isolation valve (a safety component of Hyperloop) in 2021. In 2022, Transpod has also revealed its scaled-down fully-electric vehicle, called FluxJet.

Communications is one of the essential technologies to realize Hyperloop, along with others like magnetic levitation, pod propulsion, pod and tube design, pod attitude control, etc. Especially, wireless communications is crucial for ensuring Hyperloop's safety and providing passenger convenience like on-board Internet access. In addition, in the case of emergency, the Hyperloop's control center may need to wirelessly transmit control packets (e.g., emergency slow-down) to the pods. Regarding safety, the Hyperloop system may deploy many sensors inside the tube and on the pod so that they monitor the status of travelling pods, and thus-collected data are consistently transferred to the Hyperloop control center via wireless links, as shown in Fig. 1. Regarding on-board experience, high-capacity wireless connection should be maintained to provide passengers with reliable connectivity to the outer world via Internet access.

In the literature, there have been several studies on Hyperloop communications. First, [2] presented recent developments in Hyperloop communication systems and suggested future research directions. Then, [3] proposed the 5G-based Hyperloop network adopting a tube structure with EM lens allowing external 5G signals to penetrate the tube, but showed that such an architecture cannot guarantee the safe operation of Hyperloop. In the meantime, [4] proposed the Hyperloop communication system based on a 'leaky waveguide' installed along the inside of the tube, which is acting as a leaky feeder of wireless signals. However, such a solution is not adequate for Hyperloop since it requires deploying too many repeaters along the exceptionally-long tube to compensate the leakage loss [5] and it has difficulty in controlling its signal emission individually adapted to each moving pod. On the other hand, [6] proposed an IRS(Intelligent Reflecting Surfaces)-based intra-tube network architecture, but it also requires too many IRSs installed along the tube making it hard to manage them in the harsh environment of the near-vacuum tube.

There also exist in-depth studies on EM propagation characteristics in the tube like [7], [8], [9], [10], [11], [12]. They, however, only considered a partial section of the tube and thus failed to capture the effects caused by the entire set of base-stations (BSs) and pods residing in the tube. On the other hand, our previous study in [13] has investigated the EM propagation

This work was supported by the National Research Foundation of Korea (NRF) through the Korean Government (MSIT) under Grant No. RS-2024-00420013, Research on Interdisciplinary Wireless Communication Technology for Intra-Tube High-speed Mobility.

Hyoil Kim is the corresponding author.

ISBN 978-3-903176-65-2 © 2024 IFIP

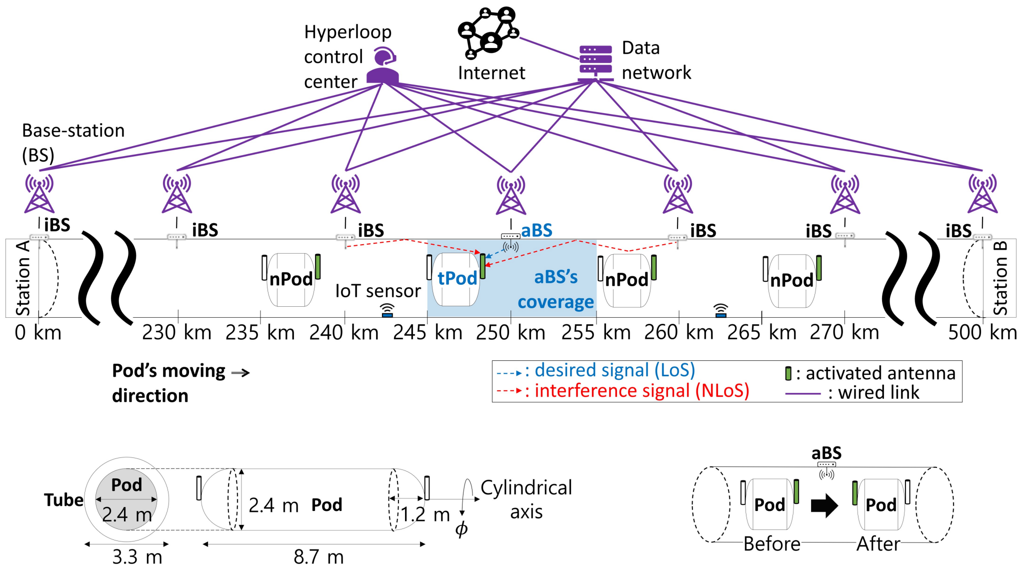

Fig. 1. Hyperloop communication system architecture

characteristics inside a 500-km-long tube with all the BSs and pods considered, while proposing a novel method to efficiently analyze the gigantic intra-tube EM environment. The paper also showed that intra-tube EM propagation analysis should mainly rely on numerical analysis (via EM simulation tools like HFSS) due to the existence of geometrically-complex and mobile discontinuities (e.g., pods) within the tube, making the intra-tube environment intractable to analyze solely through theoretical methods.

Equipped with our intra-tube EM numerical analysis methodology in [13], the logical next step is to evaluate the intra-tube wireless channel capacity and to investigate novel ways to enhance it as much as possible. In such a vein, this paper first derives the per-pod channel capacity upon utilizing the intra-tube per-pod received power profiles (for both desired and interfering signals) reported in [13], and then shows that the existing Hyperloop pod design (with a metallic exterior) cannot fulfill the channel capacity requirement to serve in-pod passengers with usual Internet traffic demand. Therefore, this paper proposes a novel pod design with an EM absorbing material coated outside the pod, and shows that such a design can help a pod to preserve the desired signal's received power from its associated BS while much suppressing the unwanted signal's power from an interfering BS. Moreover, we will show the efficacy of the proposed design in enhancing the per-pod channel capacity by optimizing the coated layer's thickness.

The paper is organized as follows. Section II introduces the Hyperloop communications system model considered in this study. Section III describes our methodology of per-pod channel capacity evaluation and its application to the metal pods (i.e., pods with a metallic exterior). Then, Section IV presents our proposed 'double-layered' pod design with an EM absorbing external layer covering a metallic inner layer, and shows that it can much enhance the per-pod channel capacity enough to satisfy the requirement for the channel capacity. Finally, the paper concludes with Section V.

II. System Model and Preliminaries

This work is a follow-up study of our recent publication in [13] which revealed the full-scale EM propagation characteristics in the Hyperloop tube. Based on the discoveries in [13], this paper analyzes the intra-tube wireless channel capacity and tries to enhance it by proposing a novel pod structure. Therefore, we closely follow the system model of [13] as shown in Fig. 1, where the Hyperloop communications system includes the metal tube connecting two end-stations A and B, multiple BSs at fixed locations, and multiple moving pods. The tube's dimensions are 500 km in length and 3.3 m in diameter, while a pod's dimensions are 8.7 m in length and 2.4 m in diameter. In addition, pods are concentric with the tube as illustrated in the lower left corner of Fig. 1. The intra-tube BS antennas are installed every 10 km (i.e., per-BS half-coverage length is 5 km), where each one is a single quarter-wavelength monopole antenna standing downwards on the inner ceiling of the tube.

Pods are assumed to depart from station A every 30 seconds, which is the minimum departure interval proposed by SpaceX [1] assuming each pod equipped with an emergency braking system. In addition, the pods are sharing the same mobility pattern such as: uniform acceleration at $0.5g$ (where g is the gravitational acceleration), traveling at the maximum speed of 1,200 km/h, uniform deceleration at $0.5g$, and arrival at station B. Moreover, each pod is associated with its closest BS at a given location, and its handover is assumed to incur insignificant delay due to its pre-determined mobility pattern (i.e., the handover process can be pre-arranged). We also assume that every pod is equipped with two antennas at its head and tail respectively so that it can only activate the one closer to its associated BS while temporarily turning off the other, as shown in the lower right corner of Fig. 1. In this way, we can avoid self-blocking of the desired signal from the associated BS.

For a pod accelerating at $0.5g$, it reaches 1,200 km/h after travelling 11.34 km from station A, which implies that pods are cruising at their maximum speed for the most part of their journey (to be precise, 95.46 % out of the total travel distance of 500 km). Hence, this paper in the sequel focuses on evaluating and enhancing the per-pod channel capacity in the dominant case of the maximum-speed travel. Then, a BS can only be associated with a single pod because both inter-BS distance and inter-pod distance become 10 km in the maximum-speed zone. This instantly implies that the communication resources of a BS within its coverage area can be exclusively utilized by the pod associated with the BS.

Furthermore, the selective antenna activation principle (i.e., a pod activates its antenna closer to the associated BS) guarantees that a pod and its associated BS always has a Line-of-Sight (LOS) path, as shown in Fig. 1 with a blue dotted arrow. In addition, due to the same relative position of each pod from its associated BS, a pod and its non-associated (thus interfering) BSs always have Non-LOS (NLOS) paths, as shown in Fig. 1 with red dotted arrows. This means that any interference signal to the pod of interest ('tPod' in Fig. 1) should pass through one or more pods until it reaches the tPod, where the pods it is passing through are mostly neighboring pods ('nPod' in Fig. 1) but sometimes the tPod itself (e.g., the red dotted interference signal coming from iBS on the left of aBS). In this case, such pods act as a 8.7-meter-long obstacle to the propagation of the interference signal.

A. Preliminaries on EM Characteristics in the Tube

In a metal circular waveguide (like the Hyperloop tube), the fields of a propagating EM wave form specific configurations satisfying the wave equation and boundary conditions given by the tube structure. Each configuration is called 'mode' and categorized into two types: TE_{mn} and TM_{mn}, $m \geq 0$, $n \geq 1$, with m and n being integers, depending on which field vector is perpendicular to the EM propagation direction.[1] The parameter m indicates the number of repetitions of the mode's field over 2π radians in ϕ, the azimuth in the cylindrical coordinate system shown in the lower left part of Fig. 1. On the other hand, the parameter n signifies the order of the solutions to the wave equation that meet the boundary conditions given by the waveguide structure.

Theoretically, there could be an infinite number of modes because we can find infinitely many possible m-n pairs. In practice, however, the number of utilizable modes is finite for the given carrier frequency of intra-tube wireless communications, since each EM mode has its own cutoff frequency only beyond which the mode's energy can be propagated along the tube. Hence, the set of (practically) existing modes consists of the modes whose cutoff frequencies are below the chosen carrier frequency. In the meantime, since the wave's power is distributed into the existing modes in the tube, per-mode power (i.e., the portion of transmit power allocated to the mode) should increase with a less number of existing modes.

[1]In the TE mode, the electric field vector is perpendicular to the EM propagation direction. On the contrary, in the TM mode, the magnetic field vector is perpendicular to it.

Mode	TE_{11}	TM_{01}	TE_{21}	TE_{01}, TM_{11}	TE_{31}	TM_{21}	TE_{41}	TE_{12}	TM_{02}
Cutoff freq. (MHz)	53.24	69.54	88.32	110.80	121.48	148.51	153.76	154.17	159.62
Per-mode Bandwidth (MHz)	22.49	13.02	7.24	3.58	2.51	0.83	0.63	0.61	0.44

TABLE I
PER-MODE CHARACTERISTICS IN THE HYPERLOOP TUBE (DERIVED IN OUR PREVIOUS WORK [13])

For the given system model, [13] has revealed that the best frequency band to utilize is $[159.62, 184.50]$ MHz so as to simultaneously minimize the number of existing EM modes to ten and maximize the bandwidth of the utilized band. Among the ten modes, only three of them turn out to be capable of providing the bandwidth of 5 MHz or larger, such as {22.49, 13.02, 7.24} MHz for {TE_{11}, TM_{01}, TE_{21}}. The per-mode bandwidth were determined differently to bound the delay spread (caused by dispersion) by 239.88 ns according to a 5G's scenario, considering the phenomenon that the energy transferring velocity of an EM wave along the cylindrical axis in the tube varies with modes and frequencies. Since communication standards like 5G usually require at least 5 MHz per-link bandwidth, we focus on such modes in what follows. Table I summarizes the ten existing modes and their characteristics (cutoff frequency and per-mode bandwidth).[2]

This paper assumes single-mode communications, i.e., only one mode is utilized at a time, to avoid excessive complexity in designing communication systems. In addition, we hereby consider downlink communications only, based on the fact that downlink traffic is getting more dominant in mobile networks, especially with today's high video traffic demand.

B. Adding More Realism to the System Model

On top of the model in [13], we have made a few adjustments in the system model as follows, to make it more realsitic. First, we assumed that the tube material is 'ASTM A516 Grade 70' which is a carbon steel with the conductivity of 5,882,353 S/m and has been used by Korea Railroad Research Institute (KRRI) for building its near-vacuum Hyperloop tube prototype in 2018 [14]. Note that [13] assumed the tube material has the conductivity of 0.139×10^{-7} S/m.

In addition, we assumed that a pod's antennas are the quarter-wavelength monopole, whose dimensions may vary according to *which EM mode to utilize* among TE_{11}, TM_{01}, TE_{21}. Particularly, the antenna radius and length of the three modes are given as {11.5, 2.8, 2.7} mm and {376.3, 395.8, 389.4} mm, respectively. Different antenna dimensions among the three modes are due to varying per-mode frequency band and fine-tuning of each monopole antenna to minimize the return loss at its carrier frequency. For each mode, the position of the antenna of a pod has been determined as illustrated in

[2]The Doppler shift caused by a moving pod is ignored because it is very small (less than 206 Hz) compared to the carrier frequencies we consider.

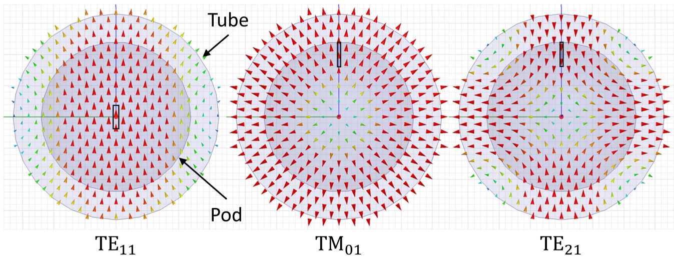

Fig. 2. Per-mode electric field pattern on tube's cross-section, with on-pod antenna location (the stronger the field, the thicker and more reddish the arrows are)

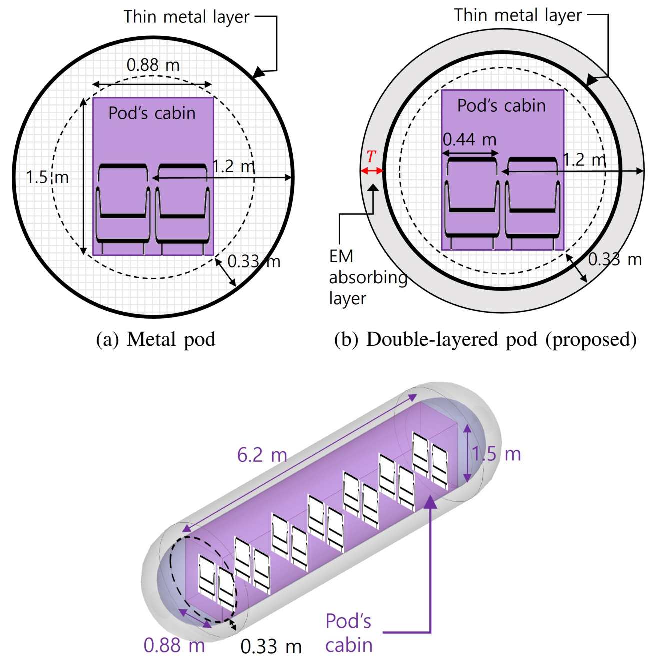

(a) Metal pod

(b) Double-layered pod (proposed)

(c) Pod's cabin within the pod (bird's-eye view)

Fig. 3. Pod structures: metal pod vs. double-layered pod

Fig. 2 to maximize the received power considering per-mode field patterns, where an antenna is drawn as a black rectangle (with an inflated size for visibility).

III. Per-pod Channel Capacity Evaluation: Methodology & Capacity of Metal Pod Structure

To evaluate the per-pod channel capacity in the Hyperloop tube, this paper considers two different pod designs. The first one is the 'metal pod' covered by a single metal layer with high conductivity, as previously considered in [13]. The second one is the 'double-layered pod' covered by a metal inner layer and an outer layer made of an EM absorbing material, which is a novel proposal of this work to enhance the channel capacity. In this section, we introduce our channel capacity evaluation methodology in Section III-A, and then present its application to the metal pod structure case in Section III-B. Later on, Section IV will introduce the channel capacity evaluation with double-layered pods and investigate how much the capacity can be enhanced by the proposed pod design.

The two types of pod structures are shown in Figs. 3a and 3b, where both of them enclose a cuboid-shaped cabin (colored in purple) with a height of 1.5m, a width of 0.88m, and a length of 6.2m as shown in Fig. 3c. The height is determined based on the top 1% sitting height of US army personnel (1m) [15] plus the seat cushion thickness (5cm) and the height of the seat off the floor (45cm). The cabin's width is set to be twice the seat width of the main cabin of the Airbus A350-900 359, with an 81-cm-long seat pitch [16]. Accordingly, each cabin can accommodate up to 14 seats.

A. Channel Capacity Evaluation Methodology

Per-pod channel capacity evaluation requires to derive the received signal power measured by the pod of interest. To obtain it, we utilized the method proposed by our previous work in [13], which *combines* a full-wave 3D EM numerical simulation via HFSS *with* a MATLAB-based multiport microwave circuit analysis, to accurately and efficiently model the EM propagation within the gigantic tube structure.[3] In the simulations, we designate one of the moving pods as 'target pod' (henceforth denoted by 'tPod'), and focus on its received signal when it is located in the left-half coverage of its 'associated BS' (henceforth denoted by 'aBS') at 250 km, as shown in Fig. 1. In addition, the pods other than tPod are called 'neighboring pods' (denoted by 'nPod'), while the BSs other than aBS are called 'interfering BSs' (denoted by 'iBS'). Note that within aBS's coverage, only tPod is associated with the aBS, since the inter-pod distance at their maximum speed is the same as the inter-BS distance of 10 km. In addition, the capacity evaluation on the left-half coverage of aBS is the same as that on the right-half coverage, due to symmetry.

We sampled tPod's trajectory every 10 ms, and at each sample time we evaluated tPod's received power of the desired signal (from the aBS) and that of the sum-interference signal (from iBSs). To obtain the received power P_{rec} (which is of either the desired signal or the sum-interference signal) by the tPod's antenna,[4] we first evaluated the received power P_{tube} on the tube's circular cross-section at the antenna's location, and then multiplied it with the power ratio of P_{rec} to P_{tube} where the ratio can be obtained through the analytical procedures introduced in [17], [18] considering the EM field components and patterns.

The downlink network traffic destined to in-pod passengers is random and unpredictable by nature, since its packets are generated at random moments. Accordingly, we assume that each iBS transmits at random times with a fixed duty cycle, while the same duty cycle value is applied to all the BSs. We tried different duty cycle values such as $\{10, 30, 50, 70, 90\}\%$, to consider diverse traffic situations and to investigate the

[3]More specifically, we partitioned the entire tube into a series of short blocks with three types (BS, pod, and empty), performed a HFSS simulation for each block type, and merged the result of such simulations with MATLAB. A BS (or pod) block is a tube section with a BS (or pod) at its mid-point. An empty block is a tube section with nothing inside.

[4]Specifically, the power received by the antenna's rectangular cross-section.

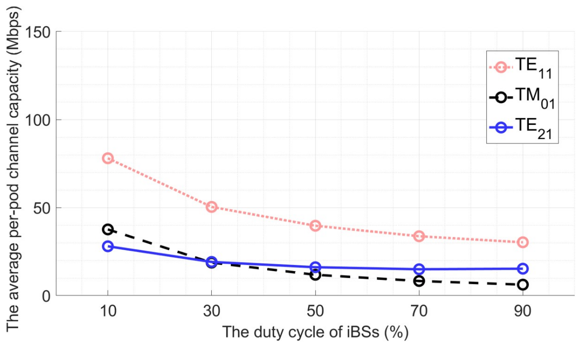

Fig. 4. The average per-pod channel capacity of the metal pod

impact of duty cycle on the per-pod channel capacity. With a given duty cycle, at each sample time we generated one thousand random realizations of combined transmission patterns of all iBSs, to observe the mean collective behavior of the randomly-transmitted interference signals. Hence, we took the average of thus-obtained one thousand sum-interference values, which will be henceforth called '*instantaneous* mean sum-interference power' to signify that it is regarding a certain sampling time.

Then, for EM mode o, duty cycle u, and sample time t, the *instantaneous* per-pod channel capacity $C_{o,u,t}$ is given as

$$C_{o,u,t} = B_o \times \log_2\left(1 + \frac{P_{o,t}}{I_{o,u,t} + N_o}\right), \tag{1}$$

where B_o is the maximum allowed bandwidth of the mode, and $P_{o,t}$ and $I_{o,u,t}$ are the desired signal power and the sum-interference power received by the tPod, respectively. Note that $P_{o,t}$ and $I_{o,u,t}$ can be obtained by P_{rec} as mentioned earlier, while $I_{o,u,t}$ is the instantaneous mean sum-interference power. In addition, $N_o = k_B T_{temp} B_o$ is the thermal noise power with the Boltzmann constant k_B and the temperature T_{temp}. This study sets the thermal noise power according to the maximum temperature of $T_{temp} = 600$ K, by referring to the existing studies on the intra-tube aerodynamics [19], [20]. This allows us to perform a conservative channel capacity analysis, and thus-derived N_o is given as $\{1.864, 1.079, 0.600\} \times 10^{-13}$ W, for TE_{11}, TM_{01}, TE_{21}, respectively.

B. Per-pod Capacity of Metal Pods

We first reveal that the metal pod design in Fig. 3a achieves an insufficient per-pod channel capacity to support today's popular video streaming services for onboard passengers. Considering that the network speed of 20 Mbps is required to provide reliable video streaming of a 4K YouTube video [21], each pod needs to achieve the channel capacity of 280 Mbps for serving 14 passengers. To check if the requirement can be fulfilled, Fig. 4 presents the *average* channel capacity of the 'metal' tPod moving in the left-half coverage of the aBS. The average is taken over time samples mapped to the half coverage such as $\sum_t C_{o,u,t}/\tau$, with τ being the number of samples involved in the summation. As can be seen, TE_{11} exhibits the best performance among the three modes regardless of the duty cycle, achieving between 30 Mbps and 80 Mbps, whereas the performance of TM_{01} and TE_{21} are always inferior than that of TE_{11}. Therefore, none of the three modes achieve the requirement of 280 Mbps.

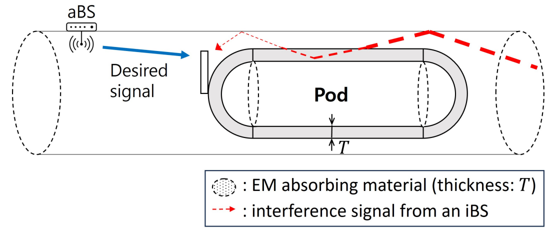

Fig. 5. The effect of the EM absorber in suppressing the interference power

In the next section, we will present our solution to achieve a much enhanced per-pod channel capacity with the double-layered pod structure.

IV. Per-pod Channel Capacity Enhancement via Double-layered Pod Structure

According to Eq. (1), we can enhance the per-pod channel capacity either by increasing the transmit power or by suppressing the sum-interference power. Increasing the transmit power of each BS, however, does not help much since it would also increase the sum-interference power equally, thus leading to a similar SNR (Signal-to-Noise Ratio). Therefore, we take an approach to suppress the sum-interference power, by proposing the double-layered pod design with an EM absorbing material coated outside.

Fig. 3b illustrates the structure of the proposed double-layered pod design that comprises an outer layer made of an EM absorbing material, an inner thin metal layer, and a core structure enclosing the pod's cabin. For the outer layer with the thickness of T, we consider either ECCOSORB MF-124 [22] (henceforth denoted by 'MF') or FAM-5GS6 [23] (henceforth denoted by 'FAM') as an EM absorbing material, whose characteristics in terms of {relative permittivity, relative permeability, dielectric loss tangent, magnetic loss tangent} are given as {40, 5.7, 0.13, 0.1} for the former and {107.28, 4.44, 0.026, 0} for the latter. Note that T should be less than 33.05 cm to allow the core to enclose the cabin, and hence we consider six possible values of T: {5, 10, 15, 20, 25, 30} cm to investigate the effect of the outer layer's thickness on the per-pod channel capacity. In addition, the thickness of the inner metal layer is assumed to be just a few millimeters, considering the typical thickness of commercial thin-walled aircrafts [24].

The double-layered pod design helps to suppress the sum-interference power by the following principles. First of all, the desired signal's propagation is much less affected by the EM absorbing layer than what the sum-interference signal's propagation experiences, because there always exists an LOS path between tPod and its aBS thanks to the selective activation of the two antennas at the tPod (as explained earlier in Section II). On the contrary, an interference signal is attenuated by the EM absoring material whenever it travels through the

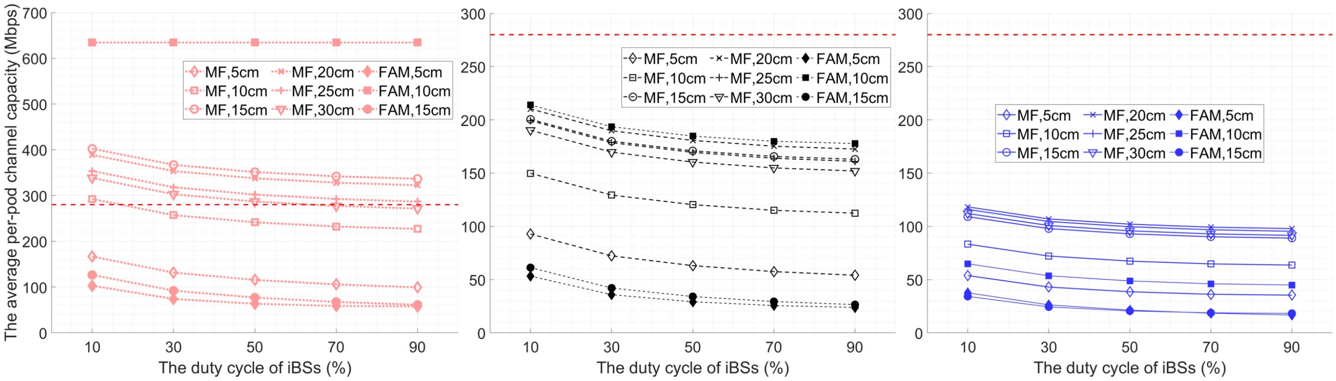

(a) TE_{11} (b) TM_{01} (c) TE_{21}

Fig. 6. The average per-pod channel capacity of the double-layered pods (the horizontal dotted line is the channel capacity requirement of 280 Mbps)

8.7-meter-long donut-like gap between an nPod and the tube, where nPods are encountered once every 10 km.

The aforementioned 'gap' consists of the vacuum and the EM absorbing material layer of the nPod. When the interference signal propagates through the EM absorbing material layer, the signal's EM fields incur the motion of free/bound charges and electric/magnetic dipoles of the EM absorbing material layer. Due to the movement, the inertial, elastic, and frictional forces cause energy loss of the signal against the motion [25]. Specifically, a fraction of the interference signal infiltrates into the EM absorbing material covering the nPod, where its energy is converted to the thermal energy, as illustrated in Fig. 5. Note that the amount of such energy conversion is determined by the thickness of the EM absorbing material because the degree of impedance mismatch depends on it. In addition, the further an iBS is located from tPod, the more attenuated the inteference signal from the iBS becomes, due to a larger number of nPods encountered by the interference signal.

Fig. 6 illustrates the evaluation result of the average per-pod channel capacity with the double-layered pod for the tPod moving in the left-half coverage of the aBS, with various T values and duty cycles. It can be seen that in every mode, the average channel capacity increases as T grows until it reaches the best performance, beyond which it starts decreasing. In particular, for MF, TE_{11} performs the best when $T = 15$ cm, whereas both TM_{01} and TE_{21} achieve the best performance when $T = 20$ cm. For FAM, every mode performs the best when $T = 10$ cm. On the other hand, regardless of EM modes and EM absorbing materials, the average channel capacity decreases as the duty cycle increases since the sum-interference power increases with more frequent iBS transmissions.

As a result, in case of MF, TE_{11} meets the requirement for all the duty cycles when $T = \{15, 20, 25\}$ cm. Specifically, when $T = 15$ cm, the average channel capacity of TE_{11} is at least 20 % (and up to 43 %) greater than the system requirement. However, TM_{01} and TE_{21} fail to meet the requirement regardless of T. Therefore, TE_{11} seems to be the only mode that can support typical mobile traffic demands, if MF is adopted.

Similarly, in case of FAM, only TE_{11} meets the requirement at all the duty cycles when $T = 10$ cm, whose average channel capacity is 126% greater than the requirement. One notable point is that the average channel capacity of TE_{11} for $T = 10$ cm is almost flat over the varying duty cycles, which is because its average sum-interference power is much weaker than in the other cases, thanks to the strong EM absorption given by the chosen EM absorbing material and its thickness, as will be shown in more details in the following subsection. As a result, SNR (which is irrelevant to the ducy cycle) becomes the dominant factor determining the average channel capacity, leading to the flat pattern.

A. In-depth Analysis on the Impact of the Proposed Pod Structure

For a deeper analysis, we further investigate the desired signal and the sum-interference signal received by the tPod traveling in the left-half coverage of the aBS. While doing so, we consider the following three cases: the metal pod structure, the double-layered pod structure with MF, and the double-layered pod structure with FAM. In the double-layered pod cases, the EM absorbing layer's thickness is optimized for each EM mode following the earlier discoveries from Fig. 6, as follows: i) MF: 15 cm for TE_{11}, 20 cm for TM_{01} and TE_{21}, and ii) FAM: 10 cm for every mode. Note that in the sequel, the power of the desired signal and the sum-interference signal are normalized by the per-BS transmit power.

1) Per-location desired signal power received by tPod: Fig. 7 represents the power of the desired signal received by the tPod for the three cases. As can be seen in Fig. 7a, the metal pod's power envelope fluctuates as the tPod travels, with the peak-to-bottom gap being more prominent in TE_{11} than in the other two modes. However, by adopting the double-layered pod structures, the fluctuation level of the three modes gets mitigated, thus making the wireless channel more reliable, as shown in Figs. 7b and 7c.

As a trade-off to the weaker fluctuation compared to the metal pod, the double-layered pod structure with the MF incurs the average desired signal power decreased by $\{5.75, 2.34\}$ dB for TE_{11} and TM_{01} respectively, whereas the average desired signal power of TE_{21} enhances a little by 0.05 dB. For the FAM case, the average desired signal power is decreased by

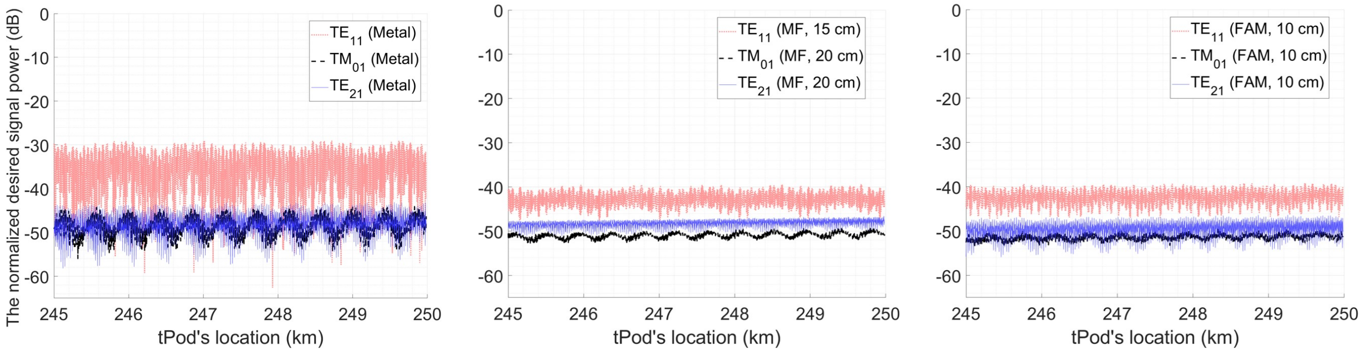

(a) Metal only (b) Metal+MF (with optimal per-mode thickness) (c) Metal+FAM (with optimal per-mode thickness)

Fig. 7. The desired signal power received by the tPod

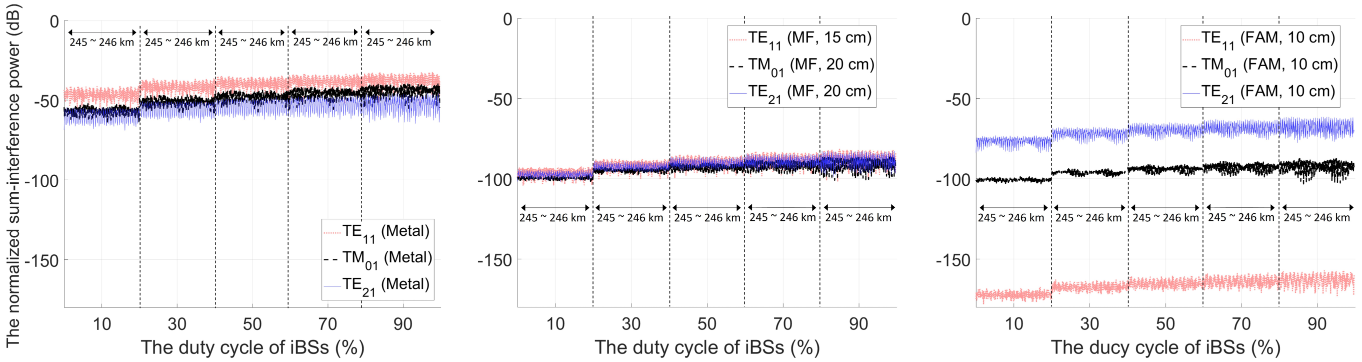

(a) Metal only (b) Metal+MF (with optimal per-mode thickness) (c) Metal+FAM (with optimal per-mode thickness)

Fig. 8. The sum-interference signal power received by the tPod located at $[245, 246]$ km

$\{5.27, 2.81, 1.3\}$ dB for TE_{11}, TM_{01}, and TE_{21}, respectively. Nevertheless, such slight reduction in the average desired signal power is surely compensated by the reduction in the average sum-interference power by the double-layered pod structure, as will be shown in Figs. 8 and 9.

2) Per-location sum-interference power received by tPod: Fig. 8 represents the normalized sum-interference power received by the tPod, while it is travelling at the locations from 245 km to 246 km. Again, we have plotted the results for the three pod structure cases along with five tested duty cycles and three EM modes, where each subfigure contains five sections along the x-axis, each corresponding to a different duty cycle value with varying locations from 245 km to 246 km. As shown, the phenomenon of power fluctuation alleviation (which was observed earlier with the desired signal) is also found in the case of the sum-interference power. Furthermore, in all three pod structures, an increasing tendency in fluctuation is observed as the duty cycle grows (despite the fact that the plots in Figs. 8a and 8b are not well distinguished among the EM modes due to the overlaps). Additionally, we can clearly see the gradual aggravation of the sum-interference power according to the increase in duty cycle, as mentioned in the discussion of Fig. 6.

3) Average sum-interference power received by tPod: Fig. 8 has also shown that the sum-interference power itself

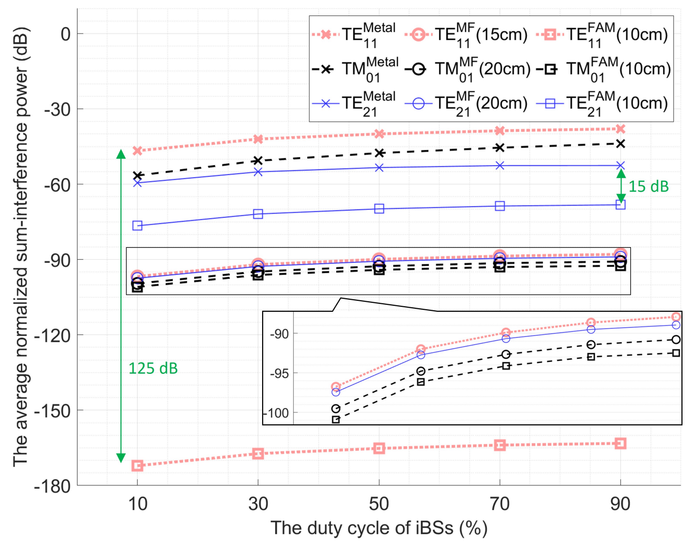

Fig. 9. The average sum-interference power received by the tPod

gets dramatically reduced by adopting the double-layered pod structures. To further investigate the benefit of the proposed pod structure, we now focus on the *average* sum-interference power received by the tPod with varying duty cycle values, as shown in Fig. 9. Note that the average is taken over the pod's travelling locations from 245 km to 250 km, i.e., the left-half coverage of its aBS.

The plots in Fig. 9 show that the average sum-interference power of the metal pod case is observed to be always larger than those of the double-layered pod cases, regardless of duty cycle and EM mode. In particular, the average sum-interference power turns out to be mitigated by at least 15 dB (for TE_{21}) and by up to 125 dB (for TE_{11}), if the double-layered pod design is adopted. Note that some of the plots have been drawn again on a larger scale in the separate box, for better readability.

4) Summary of findings: With a proper optimization of the EM absorber's thickness individually for each EM mode, the adoption of the proposed double-layered pod structure has a huge potential and benefit in enhancing the per-pod downlink channel capacity in the Hyperloop tube environment. Although the proposed design may slightly deteriorate the desired signal power, the significant reduction in the sum-interference power is more prominent and sufficient to offset the loss in the desired signal power. Specifically, the enhancement in the average sum-interference power is by more than 15 dB for any duty cycle value and EM mode, while it can be even up to 125 dB when using an optimal EM absorber setup (i.e., 10-cm-thick FAM) and a right EM mode (i.e., TE_{11}).

B. Discussion

We have only considered two EM absorbing materials due to the scarcity of EM absorbing material data which fit into our frequency band of interest. Nevertheless, the EM absorbing materials have presented evidences that coating the pod with an EM absorbing material much enhance the per-pod channel capacity. Such materials affect the electric and magnetic fields of the signal passing through pods, and their impact depends on the EM absorbing material's characteristics.

Furthermore, as far as what we have surveyed, most EM absorbing materials do not support its operating temperature up to 600 K. Therefore in the future, it is desirable and necessary for the Hyperloop industry to develop new EM absorbing materials optimized to the Hyperloop environment.

V. Conclusion

This paper proposed a novel solution to enhance the per-pod channel capacity of the Hyperloop communications system by introducing the double-layered pod structure coated with an EM absorbing material. We have first shown that the single-layered metal pod design cannot fulfill the minimum required channel capacity in provisioning 4K UHD video streaming for on-board passengers. Then, we demonstrated that the Hyperloop system with the double-layered pods can achieve the required per-pod channel capacity, thanks to the pod's outer layer absorbing the power of interference signals passing through the pod resulting in reduction of the average sum-interference power by up to 125 dB. Moreover, it is revealed that the thickness of the EM absorbing layer plays a crucial role in optimizing the per-pod channel capacity.

In future, we will further investigate how to make per-pod capacity more consistent within the aBS's coverage, possibly by adapting the transmit power according to the pod's position.

References

[1] SpaceX, "Hyperloop Alpha," white paper, 2013.

[2] W. Hedhly, O. Amin, B. Shihada, and M.-S. Alouini, "Hyperloop communications: Challenges, Advances, and Approaches," IEEE Open Journal of the Communications Society (OJ-COMS), vol. 2, pp. 2413–2435, 2021.

[3] B. Han et al., "Performance Analysis of Train-Ground Communication System for Vacuum Tube High-Speed Flying Train," in Proc. ICCC, Dec. 2021.

[4] J. Zhang et al., "Concepts on train-to-ground wireless communication system for hyperloop: Channel, network architecture, and resource management," Energies, vol. 13, no. 17, p. 4309, 2020.

[5] M. Geiger, M. Hitzler, and C. Waldschmidt, "A flexible dielectric leaky-wave antenna at 160 GHz," in Proc. EuMC, Oct. 2017.

[6] W. Hedhly et al., "Intelligent Reflecting Surfaces Assisted Hyperloop Wireless Communication Network," IEEE Transactions on Mobile Computing (TMC), vol. 23, no. 5, pp. 4943–4955, May 2024.

[7] B. Wei et al., "Field distribution characteristics of leaky-wave system in the vacuum tube for high-speed rail," in Proc. ISAPE, Dec. 2018.

[8] A. Tavsanoglu et al., "Wireless Communications in High Speed Vacuum Trains Environment for Vehicular Technology Conference," in Proc. IEEE VTC2021-Fall, Sep. 2021.

[9] ——, "Concepts of Hyperloop Wireless Communication at 1200 km/h: 5G, Wi-Fi, Propagation, Doppler and Handover," Energies, vol. 14, no. 4, p. 983, 2021.

[10] K. W. et al., "Wireless channel characterization for the high-speed flying trains in vacuum tube scenario based on propagation graph modeling theory."

[11] K. Wang, L. Liu, J. Zhan, and M. Liu, "A Novel Geometry-Based Semi-Deterministic Wideband Channel Model for Hyperloop Communications," in Proc. IEEE VTC2023-Spring, Jun. 2023.

[12] K. Wang, L. Liu, J. Zhang, M. Liu, T. Zhou, and B. Ai, "Channel characteristics analysis of millimetre-wave bands in Hyperloop scenarios based on ray-tracing," IET Microwaves, Antennas & Propagation, vol. 17, no. 8, pp. 624–633, 2023.

[13] J. Kim, H. Kim, and K. J. Han, "Hyperloop Communications: Unveiling Electromagnetic Propagation in the Hyperloop Tube," IEEE Vehicular Technology Magazine, vol. 17, no. 3, pp. 65–74, 2022.

[14] Korea Railroad Research Institute (KRRI), https://www.krri.re.kr/web/contents/krri030202.do?schM=view&id=11292, Apr. 2024, [Online].

[15] C. C. Gordon et al., "2012 Anthropometric Survey of US Army Personnel: Methods and Summary Statistics," Army Natick Soldier Research Development and Engineering Center MA, Tech. Rep., 2014.

[16] Delta Air Lines, Inc., "Airbus A350-900 Seat Specifications," https://www.delta.com/us/en/aircraft/airbus/a350, Jul. 2024, [Online].

[17] C. A. Balanis, Advanced Engineering Electromagnetics, 2nd ed. Hoboken, NJ, USA: John Wiley & Sons, Inc., 2012.

[18] D. A. Pozar, Microwave Engineering, 4th ed. Hoboken, NJ, USA: John Wiley & Sons, Inc., 2011.

[19] Y. Sui, J. Niu, Q. Yu, Y. Yuan, X. Cao, and X. Yang, "Numerical analysis of the aerothermodynamic behavior of a Hyperloop in choked flow," Energy, vol. 237, pp. 1–14, 2021.

[20] K. Zhou, G. Ding, Y. Wang, and J. Niu, "Aeroheating and aerodynamic performance of a transonic hyperloop pod with radial gap and axial channel: A contrastive study," Journal of Wind Engineering and Industrial Aerodynamics, vol. 212, pp. 1–16, 2021.

[21] Google LLC, "System Requirements and Supported Devices for YouTube," https://support.google.com/youtube/answer/78358, Apr. 2024, [Online].

[22] E&C Engineering Co., Ltd., "ECCOSORB MF Datasheet," https://ece.co.jp/assets/pdf/products/ECCOSORB%20MF_en.pdf, Apr. 2024, [Online].

[23] Crown Ferrite Enterprise Co., "High Frequency Absorbent and Thermal Conduction Composite (FAM-5GS6)," https://cfe.com.tw/2-absorber/crown-ferrite-absorber-absorbent-thermal-conduction-composite-fam5gs6.pdf, Apr. 2024, [Online].

[24] Z. Mikulik and P. Haase, "CODAMEIN - Composite Damage Metrics and Inspection (high energy blunt impact threat)," Mar. 2012, EASA.2010.C13 Final Report.

[25] M. M. Tirkey and N. Gupta, "Electromagnetic Absorber Design Challenges," IEEE Electromagnetic Compatibility Magazine, vol. 8, no. 1, pp. 59–65, 2019.